Geomechanics and Engineering, *Vol. 38, No. 3 (2024) 319-334*
https://doi.org/10.12989/gae.2024.38.3.319

A new dynamic construction procedure for deep weak rock tunnels considering pre-reinforcement and flexible primary support

Jian Zhou[1,2a], Mingjie Ma[3b], Luheng Li[3c], Yang Ding*[1,2] and Xinan Yang[3d]

[1]*Department of Civil Engineering, Hangzhou City University, Hangzhou 310015, China*
[2]*Key Laboratory of Safe Construction and Intelligent Maintenance for Urban Shield Tunnels of Zhejiang Province, Hangzhou City University, Hangzhou 310015, China*
[3]*The Key Laboratory of Road and Traffic Engineering, Ministry of Education, Tongji University, Shanghai 201804, China*

(*Received April 24, 2024, Revised June 22, 2024, Accepted July 30, 2024*)

Abstract. The current theories on the interaction between surrounding rock and support in deep-buried tunnels do not consider the form of pre-reinforcement support or the flexibility of primary support, leading to a discrepancy between theoretical solutions and practical applications. To address this gap, a comprehensive mechanical model of the tunnel with pre-reinforced rock was established in this study. The equations for internal stress, displacement, and the radius of the plastic zone in the surrounding rock were derived. By understanding the interaction mechanism between flexible support and surrounding rock, the three-dimensional construction analysis solution of the tunnel could be corrected. The validity of the proposed model was verified through numerical simulations. The results indicate that the reduction of pre-deformation significantly influences the final support pressure. The pre-reinforcement support zone primarily inhibits pre-deformation, thereby reducing the support pressure. The support pressure mainly affects the accelerated and uniform movement stage of the surrounding rock. The generation of support pressure is linked to the deformation of the surrounding rock during the accelerated movement stage. Furthermore, the strength of the pre-reinforcement zone of the surrounding rock and the strength of the shotcrete have opposite effects on the support pressure. The parameters of the pre-reinforcement zones and support materials can be optimized to achieve a balance between surrounding rock deformation, support pressure, cost, and safety. Overall, this study provides valuable insights for predicting the deformation of surrounding rock and support pressure during the dynamic construction of deep-buried weak rock tunnels. These findings can guide engineers in improving the construction process, ensuring better safety and cost-effectiveness.

Keywords: deep-buried tunnels; flexibility; mechanical model; pre-reinforcement; support pressure

1. Introduction

As the arch effect of deep-buried weak rock tunnel construction is not obvious, the surrounding rock still produces large deformation, which seriously threatens the safety of tunnel construction (Sainoki *et al.*2017, Panthi and Shrestha 2018, Sakcali and Yavuz 2019, Su *et al.* 2020, Iasiello, *et al.* 2021, Pandit and Babu 2022, Zaheri *et al.*2023). Large deformation is mainly reflected in part of the weak surrounding rock section due to the support is difficult to timely easy to appear vault instability. Currently, the commonly adopted method is to use the form of pre-reinforcement of overrun grouting to inhibit the pre-deformation, coupled with the primary support in the form of rockbolt-shotcrete-steel arch to inhibit the deformation of the surrounding rock at the back of the excavation surface, so as to avoid the occurrence of the instability situation (Dehghan *et al.* 2012, Wong *et al.* 2013, Sun *et al.* 2021, Showkati *et al.* 2021, Zaid 2021, Mirzaeiabdolyousefi *et al.* 2022). However, with the complexity of the form of support, the dynamic relationship of "support-surrounding rock" becomes more and more intricate (Zhou *et al.* 2023a,,b, Zhou *et al.* 2024). It will inevitably lead to a lot of doubts about the mechanical evolution mechanism of support-surrounding rock in weak rock tunnels.

The mechanical evolution law of surrounding rock-support is the core problem of tunnel theory analysis. Currently, academics mainly carry out the analysis from the interaction between the surrounding rock and the support behind the excavation surface. *Sun et al.* (2023) proposed an analytical model to analyze the entire process of support-surrounding rock interaction in an underwater mined tunnel considering the combined effect of blasting damage and seepage pressure. Chu *et al.* (2023) presented a time-dependent solution for deeply buried supported circular tunnels excavated in viscoelastic-plastic strain-softening rock masses, in which both the whole process of longitudinal excavation and the sequential installation of two elastic linings are considered. Some scholars also reflect the interaction between the surrounding rock and the support through the Convergence-Confinement Method (CCM). Lee *et al.* (2020) used Convergence-Confinement

*Corresponding author, Ph.D.
E-mail: ceyangding@zju.edu.cn
[a]Ph.D.
[b]Ph.D.
[c]Ph.D.
[d]Professor

ISSN: 2005-307X (Print), 2092-6219 (Online)

Method in conventional tunneling at a preliminary stage of the support design. They postulated a circular tunnel through the ground in an initially isotropic stress state and the behavior of ground-support interaction simplified utilizing a two-dimensional plane-strain. Wang *et al*. (2021) used the CCM approach to determine the support performance of a Steel-Concrete Composite Support (SCCS) system, which is characterized by an improved stiffness of the primary support due to its unique arch type (pi-type) and construction steps. It was not difficult to find that the above researches have matured the theory of support interaction between the surrounding rock and the back of the excavation face, but the theory of considering the surrounding rock pre-reinforcement was rarely reported. Thus, the mechanical evolution of the surrounding rock-support regarding the consideration of pre-reinforcement forms still needs to be further extended.

Furthermore, while there has been considerable research on the analytical solution for the evolution prediction of surrounding rock deformation and the role of support, there has been limited investigation into support pressure. Only a few scholars have undertaken studies in this area. Cui et al. (2015) solved for the virtual support pressure in a circular tunnel with a hydrostatic initial stress field. Yan et al. (2018) used the convergence-confinement method to solve the analytical solution of the anchor support problem in expansive soils to obtain the characteristic curves of the surrounding rock in anchor-reinforced expansive loess tunnels. Shen *et al.* (2019) divided the convergence-confinement method into two stages and proposed an improved method for calculating lining pressure and deformation. It is thought that reducing the final pressure on the lining could be achieved by reducing the lining stiffness and delaying the installation time. Ghorbani *et al.* (2018) used two different types of artificial neural networks (ANNs) to predict the P-i of circular tunnels in elasto-plastic, strain-softening rock mass. However, the current support pressure calculation and field measured value gap is too large. Measured support pressure is generally between tens of kPa and 1 MPa, but the theoretical calculation is generally several MPa or even more than ten MPa. It is clear that there is no primary support regarded as flexible support due to a large discrepancy with the measured values. Thus, currently, there is a theoretical bottleneck in the calculation of support pressure in deep-buried tunnels, and there is an urgent need to have a comprehensive understanding of the formation mechanism of surrounding rock deformation and support pressure, so as to improve the existing method of calculating support pressure.

It is well known that support pressure arises due to deformation of the surrounding rock. In order to clarify the formation mechanism of support pressure, it is necessary to grasp the formation process of surrounding rock deformation (Wang *et al.* 2021, Li *et al*. 2023). Surrounding rock deformation is not only generated after tunnel excavation, but also in a longitudinal range in front of the excavation face. This phenomenon is generally referred to as the spatial effect of the excavation surface (Wang *et al.* 2019, Ye *et al*. 2021, Cheng *et al.* 2023). The longitudinal deformation curve of surrounding rock generally indicates the state of accelerated deformation-uniform deformation-decelerated deformation. According to Newton's second law, when an object moves with acceleration or deceleration or with uniform velocity, the thrust force acting on the object increases, decreases and remains constant, respectively. Newton's second law also applies to the surrounding rock and supporting structures. Therefore, the support pressure is only increased when the surrounding rock carries out accelerated movement, then the energy to generate the support pressure seems to have been accumulated in front of the excavation. Numerous scholars have analyzed the support pressures to be consistent with the field monitoring paths, which inevitably results in support pressures being generated for every millimetre of surrounding rock deformation acting on the support structure. Due to the high stiffness of the support structure, the support pressure must be exaggerated. Zhang and Chen (2016) attempted to correct the drawbacks of the existing calculation of support loads by establishing a conceptual model for the kinetic analysis of surrounding rock deformation based on Newton's second law, but did not give a quantitative formula for the calculation of support pressure in specific deeply buried tunnels. Thus, the pressure calculation of flexible support in deep-buried tunnels still has much room for development. In summary, there is an urgent need to propose a new procedure for calculating the construction of deep-buried tunnels considering pre-reinforcement and flexible support for deep-buried tunnels in which the excavation face has a large safety risk of weak surrounding rocks.

Thus, this study intended to propose a mechanical model of the surrounding rock pre-reinforcement form, and carry out the theoretical derivation of the stress and deformation of the surrounding rock of the deep-buried tunnel.

From the perspective of the movement of the surrounding rock deformation, the flexible characteristics of the primary support were explored, and the final analytical solution for the improvement of the construction of deep-buried soft rock tunnels was proposed. It was intended to provide theoretical support for the prediction and optimization of deep-buried weak rock tunnel construction.

2. Mechanical modeling

The following basic assumptions are proposed in this study to analyze the support loads in deep-buried tunnels under pre-reinforcement.

(1) The tunnel section is circular and its radius is r_0.

(2) The surrounding rock, pre-reinforcement and primary support materials are homogeneous, continuous and isotropic.

(3) The primary support remains in an elastic state throughout the tunneling process.

(4) The in-situ stress of the tunnel in a two-dimensional plane is equal to the overlying rock load.

The tunnel boring schematic can be shown in Fig. 1. X is the distance of the longitudinal tunnel construction from the excavation face, and the primary support is installed c

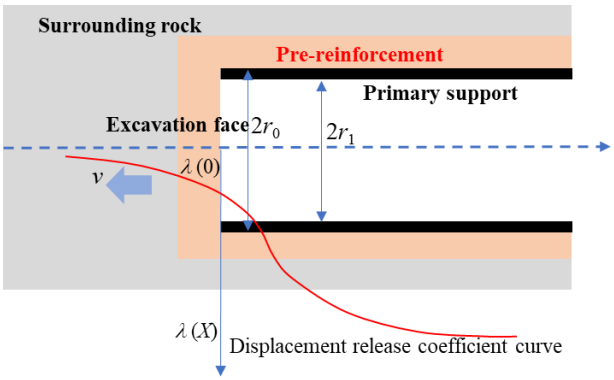

Fig. 1 Schematic diagram of conventional surrounding rock deformation and support pressure changes

immediately after the excavation face. The inner radius of the primary support after installation is r_1. v is the tunnel boring speed. $\lambda(X)$ is defined as the stress release coefficient, the stress release coefficient for the excavation face is $\lambda(0)$. $\lambda(X)$ can generally be written as (Bian *et al.* 2013, Zhao *et al.* 2016)

$$\lambda(X)=1-\alpha e^{-X/R_L} \tag{1}$$

where α is defined as the initial stress release parameter, and the value of α is in the range of 0.55 to 0.75. R_L denote the influence radius of the excavation face.

The surrounding rock has a certain self-support capacity, so as not to have large deformation before the support after the excavation of the surrounding rock. The self-support load of the surrounding rock is generally called the virtual support force, which can be expressed as (Carranza-Torres *et al.* 2013)

$$p_a(X)=\left[1-\lambda(X)\right]p_0 \tag{2}$$

The mechanical model is different from the previous two-stage model or three-stage model of the surrounding rock. In this study, the pipe sheds or ahead grouting small tubes are considered as the pre-reinforcement. With the evolution of the plastic zone, the tunneling process will produce the following three conditions. Case 1: the plastic zone is within the pre-reinforcement zone. Case 2: the plastic zone is beyond the pre-reinforcement zone, but within the anchorage range. Case 3: the plastic zone is beyond the anchorage range. Since this study mainly focuses on weak rock, the extent of the plastic zone is finally consistent with Case 3.

3. Derivation of stresses and displacements in the surrounding rock of deep-buried tunnels

3.1 Case 1

For Case 1, the surrounding rock can be divided into unanchored elastic zone, anchored elastic zone, anchored elastic reinforcement zone and anchored plastic reinforcement zone. When the stress releasing coefficient for tunneling is considered, the displacement in the unanchored elastic zone can be expressed as (Zareifard 2020)

$$\begin{cases}\sigma_r^{e1}(r,X)=\lambda(X)p_0\left[1-\dfrac{L_0^2}{r^2}\right]+\sigma_{rL_0}\dfrac{L_0^2}{r^2}\\ \sigma_\theta^{e1}(r,X)=\lambda(X)p_0\left[1+\dfrac{L_0^2}{r^2}\right]-\sigma_{rL_0}\dfrac{L_0^2}{r^2}\\ u^{e1}(r,X)=\dfrac{(1+\mu)\left[\lambda(X)p_0-\sigma_{rL_0}\right]}{E}\dfrac{L_0^2}{r}\end{cases} \tag{3}$$

where σ_r^{e1} and σ_θ^{e1} are radial and tangential stresses in the unanchored elastic zone, respectively. u^{e1} is the displacement of the unanchored elastic zone. r indicates the distance from a point in the surrounding rock to the center of the tunnel. E and μ are the modulus of elasticity and Poisson's ratio of the surrounding rock, respectively. σ_{rL_0} represents the radial stress at the junction of the anchored elastic zone and the anchored elastic zone. L_0 represents the distance between the distal end of the bockbolts and the center of the tunnel.

The anchored elastic zone acts as a composite homogeneous carrier, and its equilibrium differential equation is generally written as

$$\frac{\mathrm{d}\sigma_r^{e2}(r,X)}{\mathrm{d}r}+\frac{\sigma_r^{e2}(r,X)}{r}=\frac{\sigma_\theta^{e2}(r,X)}{r} \tag{4}$$

where σ_r^{e2} and σ_θ^{e2} represent the radial and tangential stresses in the anchored elastic zone, respectively.

The relationship between stress and displacement in the anchored elastic zone is as follows.

$$\begin{cases}\sigma_r^{e2}(r,X)=\dfrac{E_1(1-\mu_1)}{(1+\mu_1)(1-2\mu_1)}\left(\dfrac{\mathrm{d}u^{e2}(r,X)}{\mathrm{d}r}+\dfrac{\mu_1}{1-\mu_1}\dfrac{u^{e2}(r,X)}{r}\right)\\ \sigma_\theta^{e2}(r,X)=\dfrac{E_1(1-\mu_1)}{(1+\mu_1)(1-2\mu_1)}\left(\dfrac{u^{e2}(r,X)}{r}+\dfrac{\mu_1}{1-\mu_1}\dfrac{\mathrm{d}u^{e2}(r,X)}{\mathrm{d}r}\right)\end{cases} \tag{5}$$

where u^{e2} is the displacement of the anchored elastic zone. E_1 and μ_1 are the modulus of elasticity and Poisson's ratio of the anchored elastic zone, respectively. The elastic modulus of the equivalent material in the elastic zone of the anchorage is affected by the combined effect of the elastic modulus of the rock and the elastic modulus of the rockbolts, E_1 which can be written as

$$E_1=\frac{E_b\pi r_b^2+E\left(s_1s_2-\pi r_b^2\right)}{s_1s_2} \tag{6}$$

where E_b and E represent the elastic modulus of the rockbolt and rock. r_b is the radius of the rockbolt. s_1 and s_2 indicate the spacing and row spacing for rockbolt installation, respectively.

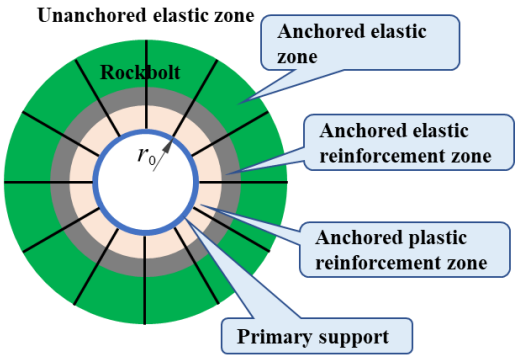

(a) Case 1

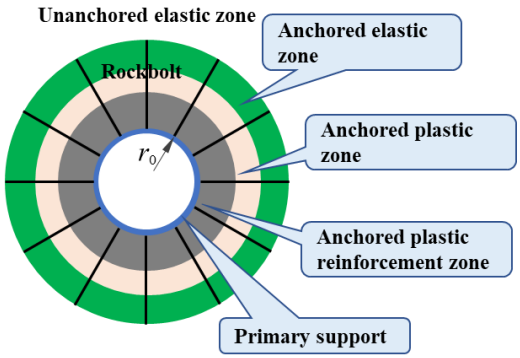

(b) Case 2

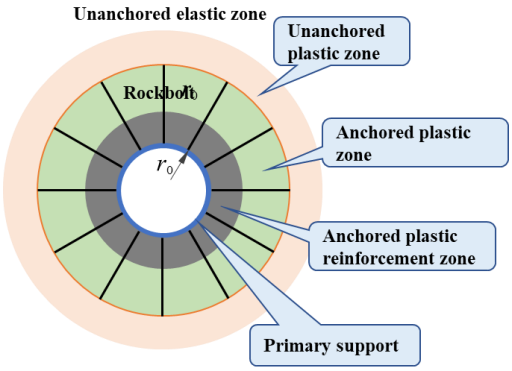

(c) Case 3

Fig.2 Mechanical models

Combining Eqs. (4) and (5), and the displacement and radial continuity at the junction of the anchored and unanchored elastic zones, an analytical general solution for the displacement of the anchored elastic zone can be obtained. The boundary equations can be given by

$$\sigma_r^{\mathrm{e}2}(L_0,X)=\sigma_{rL_0},\ u^{\mathrm{e}1}(L_0,X)=u^{\mathrm{e}2}(L_0,X) \tag{7}$$

In turn, the deformation of the surrounding rock in the anchored elastic zone can be obtained as

$$u^{\mathrm{e}2}(r,X)=\frac{u^{\mathrm{e}1}(L_0,X)(1-H_1L_0)+\frac{L_0}{H_2}\sigma_{rL_0}}{2L_0}r+\frac{u^{\mathrm{e}1}(L_0,X)(1+H_1L_0)-\frac{L_0}{H_2}\sigma_{rL_0}}{\left(\frac{2+H_1L_0}{L_0}-H_1\right)r} \tag{8}$$

where $H_1=\dfrac{\mu_1}{1-\mu_1}$. $H_2=\dfrac{E_1(1-\mu_1)}{(1+\mu_1)(1-2\mu_1)}$.

Substituting Eq. (8) into Eq. (5), the stress expressions can be obtained as respectively

$$\begin{cases}\sigma_r^{\mathrm{e}2}(r,X)=H_3+(H_1-1)\dfrac{u^{\mathrm{e}1}(L_0,X)(1+H_1L_0)H_2-L_0\sigma_{rL_0}}{\left(\frac{2+H_1L_0}{L_0}-H_1\right)r^2}\\ \sigma_\theta^{\mathrm{e}2}(r,X)=H_3+(1-H_1)\dfrac{u^{\mathrm{e}1}(L_0,X)(1+H_1L_0)H_2-L_0\sigma_{rL_0}}{\left(\frac{2+H_1L_0}{L_0}-H_1\right)r^2}\end{cases} \tag{9}$$

where $H_3=\dfrac{u^{\mathrm{e}1}(L_0,X)(1-H_1L_0)H_2+L_0\sigma_{rL_0}}{2L_0}(1+H_1)$.

The outer radius of the pre-reinforcement zone can be set as l_0. The surrounding rock displacements and stresses in the anchored elastic pre-reinforcement zone are similar to the derivation process of the anchored elastic zone, then the displacements and stresses in the zone can be written as

$$\begin{cases}u^{\mathrm{e}3}(r,X)=\dfrac{u^{\mathrm{e}2}(l_0,X)(1-H_1l_0)+\frac{l_0}{H_4}\sigma_r^{\mathrm{e}2}(l_0,X)}{2l_0}r+\dfrac{u^{\mathrm{e}2}(l_0,X)(1+H_1l_0)-\frac{l_0}{H_4}\sigma_r^{\mathrm{e}2}(l_0,X)}{\left(\frac{2+H_1L_0}{l_0}-H_1\right)r}\\ \sigma_r^{\mathrm{e}3}(r,X)=H_5+(H_1-1)\dfrac{u^{\mathrm{e}2}(l_0,X)(1+H_1l_0)H_4-l_0\sigma_r^{\mathrm{e}2}(l_0,X)}{\left(\frac{2+H_1l_0}{l_0}-H_1\right)r^2}\\ \sigma_\theta^{\mathrm{e}3}(r,X)=H_5+(1-H_1)\dfrac{u^{\mathrm{e}2}(l_0,X)(1+H_1l_0)H_4-l_0\sigma_r^{\mathrm{e}2}(l_0,X)}{\left(\frac{2+H_1l_0}{l_0}-H_1\right)r^2}\end{cases} \tag{10}$$

where $H_4=\dfrac{E_2(1-\mu_2)}{(1+\mu_2)(1-2\mu_2)}$. E_2 and μ_2 are the equivalent elastic modulus and Poisson's ratio of the rockbolt and the pre-reinforcement structure, respectively. $H_5=\dfrac{u^{\mathrm{e}2}(l_0,X)(1-H_1l_0)H_2+l_0\sigma_r^{\mathrm{e}2}(l_0,X)}{2l_0}(1+H_1)$. E_2 can be expressed as

$$E_2=\frac{E_{\mathrm{b}}\pi r_{\mathrm{b}}^2+E_{\mathrm{p}}\left(s_1s_2-\pi r_{\mathrm{b}}^2\right)}{s_1s_2} \tag{11}$$

where E_{p} is the elastic modulus of the pre-reinforcement zone.

The Mor-Coulomb strength criterion is proposed to be used for the anchored plastic reinforcement zone, then the yield equation for the anchored plastic reinforcement zone can be as follows.

$$\sigma_\theta^{\mathrm{p1}} = K_{\mathrm{p1}}\sigma_r^{\mathrm{p1}} + \sigma_{\mathrm{c}}^{\mathrm{p1}} \tag{12}$$

where $\sigma_\theta^{\mathrm{p1}}$ and σ_r^{p1} are the tangential and radial stresses in the anchored plastic reinforcement zone, respectively. $K_{\mathrm{p1}} = \left(1+\sin\varphi^{\mathrm{p1}}\right)/\left(1-\sin\varphi^{\mathrm{p1}}\right)$. $\sigma_{\mathrm{c}}^{\mathrm{p1}}$ is the uniaxial compressive strength of the anchored plastic reinforcement zone, which can generally be written as $\sigma_{\mathrm{c}}^{\mathrm{p1}} = \left(2c^{\mathrm{p1}}\cos\varphi^{\mathrm{p1}}\right)/\left(1-\sin\varphi^{\mathrm{p1}}\right)$. The surrounding rock traversed by the rockbolts are installed as a composite carrier, the composite being a homogeneous and continuous equivalent material with enhanced strength parameters. c^{p1} and φ^{p1} are the equivalent cohesion and internal friction angle in the anchored plastic reinforcement zone, respectively. According to Indraratna and Kaiser's (1990) analysis, c^{p1} and φ^{p1} have the following expressions.

$$\begin{cases} \varphi^{\mathrm{p1}} = \arcsin\left[\dfrac{\left(1+\sin\varphi_1\right)\beta + 2\sin\varphi_1}{\left(1+\sin\varphi_1\right)\beta + 2}\right] \\ c^{\mathrm{p1}} = \dfrac{c_1\left(1+\beta\right)\left(1-\sin\varphi^{\mathrm{p1}}\right)\cos\varphi_1}{\left(1-\sin\varphi_1\right)\cos\varphi^{\mathrm{p1}}} \end{cases} \tag{13}$$

where c_1 and φ_1 are the cohesion and angle of internal friction angle in the pre-reinforcement zone, respectively. β is the density parameter of the rockbolt, which can be given by

$$\beta = \frac{\pi d\eta r_0}{s_1 s_2} \tag{14}$$

where d is the diameter of the rockbolt. η represents the coefficient of friction between the rockbolts and the rock, which is related to the roughness of the rockbolts' surface. $\eta = \tan\dfrac{\varphi}{2}$ (Osgoui 2006) when non-threaded rockbolts can be used, and φ is the internal friction angle of rock. η shall equal $\tan\varphi$ while threaded rockbolts are used.

Referring to Eq. (4), the equilibrium differential equation for the anchored plastic reinforcement zone can be written as

$$\frac{\mathrm{d}\sigma_r^{\mathrm{p1}}\left(r,X\right)}{\mathrm{d}r} + \frac{\sigma_r^{\mathrm{p1}}\left(r,X\right)}{r} = \frac{\sigma_\theta^{\mathrm{p1}}\left(r,X\right)}{r} \tag{15}$$

The radius of the plastic zone in the pre-reinforcement zone can be set to R_{p}. By associating Eq. (12) with Eq. (15) and combining it with the boundary equation $\sigma_r^{\mathrm{e3}}\left(R_{\mathrm{p}},X\right) = \sigma_r^{\mathrm{p1}}\left(R_{\mathrm{p}},X\right)$, the radial stress in the anchored plastic reinforcement zone can be obtained as

$$\sigma_r^{\mathrm{p1}}\left(r,X\right) = \left(\sigma_r^{\mathrm{e3}}\left(R_{\mathrm{p}},X\right) - \frac{\sigma_{\mathrm{c}}^{\mathrm{p1}}}{1-K_{\mathrm{p1}}}\right)\left(\frac{R_{\mathrm{p}}}{r}\right)^{1-K_{\mathrm{p1}}} + \frac{\sigma_{\mathrm{c}}^{\mathrm{p1}}}{1-K_{\mathrm{p1}}} \tag{16}$$

Substituting Eq. (10) into Eq. (16), $\sigma_r^{\mathrm{p1}}\left(r,X\right)$ can be solved.

Pre-reinforcement zone, which is much stronger than weak rock, do not have significant softening characteristics. However, the dilatancy effect of the pre-reinforcement zone can be considered. The following relationship exists for the strain in the anchored plastic reinforcement zone.

$$\begin{cases} \varepsilon_r = \mathrm{d}u/\mathrm{d}r, \varepsilon_\theta = u/r \\ \varepsilon_r = \varepsilon_r^{\mathrm{e3}}\left(R_{\mathrm{p}},\ X\right) + \Delta\varepsilon_r^{\mathrm{p1}}, \varepsilon_\theta = \varepsilon_\theta^{\mathrm{e3}}\left(R_{\mathrm{p}},\ X\right) + \Delta\varepsilon_\theta^{\mathrm{p1}} \\ \Delta\varepsilon_r^{\mathrm{p1}} + \eta_1\Delta\varepsilon_\theta^{\mathrm{p1}} = 0 \end{cases} \tag{17}$$

where ε_θ and ε_r are the tangential and radial strains at a point in the surrounding rock, respectively. $\Delta\varepsilon_r^{\mathrm{p1}}$ and $\Delta\varepsilon_\theta^{\mathrm{p1}}$ are the radial and tangential strain increments in the anchored plastic reinforcement zone, respectively. η_1 is the expansion factor for the anchored plastic reinforcement zone. In the absence of pre-reinforcement, the dilatancy coefficient η_1 of the broken rock zone is 1.3 to 1.5, which should result in a plastic situation without rupture. In this case, η_1 can be taken as 1.1.

Combining Eqs. (17) and (10), and according to the boundary condition $u^{\mathrm{e3}}\left(R_{\mathrm{p}},X\right) = u^{\mathrm{p1}}\left(R_{\mathrm{p}},X\right)$, the displacement of the anchored plastic reinforcement zone can be obtained as

$$u^{\mathrm{p1}}\left(r,X\right) = u^{\mathrm{e3}}\left(R_{\mathrm{p}},X\right)\left(\frac{R_{\mathrm{p}}}{r}\right)^{\eta_1} + \frac{\eta_1-1}{r^{\eta_1}}\left[\frac{u^{\mathrm{e2}}\left(l_0,X\right)\left(1-H_1l_0\right) + \frac{l_0}{H_4}\sigma_r^{\mathrm{e2}}\left(l_0,X\right)}{2l_0\left(\eta_1+1\right)}\left(r^{1+\eta_1} - R_{\mathrm{p}}^{1+\eta_1}\right)\right.$$
$$\left. + \frac{u^{\mathrm{e2}}\left(l_0,X\right)\left(1+H_1l_0\right) - \frac{l_0}{H_4}\sigma_r^{\mathrm{e2}}\left(l_0,X\right)}{\left(\frac{2+H_1L_0}{l_0} - H_1\right)\left(\eta_1-1\right)}\left(r^{\eta_1-1} - R_{\mathrm{p}}^{\eta_1-1}\right)\right] \tag{18}$$

3.2 Case 2

The surrounding rock is divided into unanchored elastic zone, anchored elastic zone, anchored plastic zone and anchored plastic reinforcement zone. Since the stresses and displacements of the elastic and anchored elastic zones in Case 2 are the same as those in Case 1, the stress displacements and displacements of their elastic zones are the same as those in Eq. (3). The stresses and displacements in the anchored elastic zone are consistent with Eqs. (8) and (9), respectively.

The method of solving for stress and displacement in the anchored plastic zone is similar to that of Case 1. However, it is worth noting that the parameters within the anchored plastic zone are different from the anchored plastic reinforcement zone in Case 1. The radial and tangential stresses in the zone can be given by

$$\begin{cases} \sigma_r^{\mathrm{p2}}\left(r,X\right) = \left(\sigma_r^{\mathrm{e2}}\left(R_{\mathrm{p}},X\right) - \dfrac{\sigma_{\mathrm{c}}^{\mathrm{p2}}}{1-K_{\mathrm{p2}}}\right)\left(\dfrac{R_{\mathrm{p}}}{r}\right)^{1-K_{\mathrm{p2}}} + \dfrac{\sigma_{\mathrm{c}}^{\mathrm{p2}}}{1-K_{\mathrm{p2}}} \\ \sigma_\theta^{\mathrm{p2}}\left(r,X\right) = K_{\mathrm{p2}}\sigma_r^{\mathrm{p2}}\left(r,X\right) + \sigma_{\mathrm{c}}^{\mathrm{p2}} \end{cases} \tag{19}$$

where $\sigma_\theta^{\mathrm{p2}}$ and σ_r^{p2} are the tangential and radial stresses in the plastic zone of the anchorage, respectively. $K_{\mathrm{p2}}=\left(1+\sin\varphi^{\mathrm{p2}}\right)/\left(1-\sin\varphi^{\mathrm{p2}}\right)$. $\sigma_{\mathrm{c}}^{\mathrm{p2}}$ is the uniaxial compressive strength of the anchored plastic zone, which can generally be written as $\sigma_{\mathrm{c}}^{\mathrm{p2}}=\left(2c^{\mathrm{p2}}\cos\varphi^{\mathrm{p2}}\right)/\left(1-\sin\varphi^{\mathrm{p2}}\right)$. c^{p1} and φ^{p1} are the equivalent cohesion and internal friction angle in the plastic zone of the anchorage, respectively, expressed as follows

$$\begin{cases}\varphi^{\mathrm{p2}}=\arcsin\left[\dfrac{\left(1+\sin\varphi\right)\beta+2\sin\varphi}{\left(1+\sin\varphi_1\right)\beta+2}\right]\\ c^{\mathrm{p2}}=\dfrac{c\left(1+\beta\right)\left(1-\sin\varphi^{\mathrm{p2}}\right)\cos\varphi}{\left(1-\sin\varphi\right)\cos\varphi^{\mathrm{p2}}}\end{cases}\tag{20}$$

where c is the cohesion of the surrounding rock.

Similar to the calculation method in Eq. (18), the deformation of the surrounding rock $u^{\mathrm{p2}}\left(r,X\right)$ in the anchored plastic zone can be written as

$$u^{\mathrm{p2}}\left(r,X\right)=u^{\mathrm{e2}}\left(R_{\mathrm{p}},X\right)\left(\frac{R_{\mathrm{p}}}{r}\right)^{\eta_2}+\frac{\eta_2-1}{r^{\eta_2}}\left[\frac{u^{\mathrm{e1}}\left(L_0,X\right)\left(1-H_1L_0\right)+\dfrac{L_0}{H_2}\sigma_{rL_0}}{2L_0\left(\eta_1+1\right)}\left(r^{1+\eta_2}-R_{\mathrm{p}}^{1+\eta_2}\right)\right.$$
$$\left.+\frac{u^{\mathrm{e1}}\left(L_0,X\right)\left(1+H_1L_0\right)-\dfrac{L_0}{H_2}\sigma_{rL_0}}{\left(\dfrac{2+H_1L_0}{L_0}-H_1\right)\left(\eta_1-1\right)}\left(r^{\eta_2-1}-R_{\mathrm{p}}^{\eta_2-1}\right)\right]\tag{21}$$

where η_2 is the dilatancy coefficient of the anchored plastic zone.

The surrounding rock stresses and radial displacements in the anchored plastic reinforcement zone are similar to Eqs. (16) and (18) and can be expressed as

$$\begin{cases}\sigma_r^{\mathrm{p1}}\left(r,X\right)=\left(\sigma_r^{\mathrm{p2}}\left(l_0,X\right)-\dfrac{\sigma_{\mathrm{c}}^{\mathrm{p1}}}{1-K_{\mathrm{p1}}}\right)\left(\dfrac{l_0}{r}\right)^{1-K_{\mathrm{p1}}}+\dfrac{\sigma_{\mathrm{c}}^{\mathrm{p1}}}{1-K_{\mathrm{p1}}}\\ \sigma_\theta^{\mathrm{p1}}\left(r,X\right)=K_{\mathrm{p1}}\sigma_r^{\mathrm{p1}}\left(r,X\right)+\sigma_{\mathrm{c}}^{\mathrm{p1}}\\ u^{\mathrm{p1}}\left(r,X\right)=r^{-\eta_1}\left(l_0^{\eta_1}u^{\mathrm{p2}}\left(l_0,X\right)-\dfrac{H_6}{1+\eta_1}l_0^{1+\eta_1}+\dfrac{H_6}{1+\eta_1}r^{1+\eta_1}\right)\end{cases}\tag{22}$$

where $H_6=\left.\dfrac{\partial u^{\mathrm{p2}}\left(r,X\right)}{\partial r}\right|_{r=l_0}+\eta_1\left.\dfrac{u^{\mathrm{p2}}\left(r,X\right)}{r}\right|_{r=l_0}$.

In Case 2, as the radius of the plastic zone expands further than in Case 1, it should be larger than in Case 1, which is 1.2 (Wang 2013). η_2 is the dilatancy coefficient of the anchored plastic zone, which should be less than η_1, so η_2 should be 1.1.

3.3 Case 3

The surrounding rock is divided into unanchored elastic zone, unanchored plastic zone, anchored plastic zone, and anchored plastic reinforcement zone. The stress and displacement of the elastic zone in Case 3 is the same as that in Case 1, then the stress displacement and displacement of the elastic zone is the same as that in Eq. (3). The stress in the unanchored plastic zone is similar to Eq. (19) which can be expressed as

$$\begin{cases}\sigma_r^{\mathrm{p3}}\left(r,X\right)=\left(\sigma_r^{\mathrm{e1}}\left(R_{\mathrm{p}},X\right)-\dfrac{\sigma_{\mathrm{c}}}{1-K_{\mathrm{p3}}}\right)\left(\dfrac{R_{\mathrm{p}}}{r}\right)^{1-K_{\mathrm{p3}}}+\dfrac{\sigma_{\mathrm{c}}}{1-K_{\mathrm{p3}}}\\ \sigma_\theta^{\mathrm{p3}}\left(r,X\right)=K_{\mathrm{p3}}\sigma_r^{\mathrm{p3}}\left(r,X\right)+\sigma_{\mathrm{c}}\end{cases}\tag{23}$$

where $\sigma_\theta^{\mathrm{p3}}$ and σ_r^{p3} are the tangential and radial stresses in the unanchored plastic zone, respectively. $K_{\mathrm{p3}}=\left(1+\sin\varphi\right)/\left(1-\sin\varphi\right)$. σ_{c} is the uniaxial compressive strength of the rock mass, which can generally be written as $\sigma_{\mathrm{c}}=\left(2c\cos\varphi\right)/\left(1-\sin\varphi\right)$.

The deformation of the surrounding rock in the unanchored plastic zone $u^{\mathrm{p3}}\left(r,X\right)$ can be written as

$$u^{\mathrm{p3}}\left(r,X\right)=r^{-\eta_3}\left(R_{\mathrm{p}}^{\eta_3}u^{\mathrm{e1}}\left(R_{\mathrm{p}},X\right)-\frac{\left(1+\mu\right)\left[\lambda\left(X\right)p_0-\sigma_{rR_{\mathrm{p}}}\right]\left(\eta_3-1\right)}{E}\left(R_{\mathrm{p}}^{1+\eta_3}-r^{1+\eta_3}\right)\right)\tag{24}$$

where η_3 is dilatancy coefficient of the unanchored plastic zone. $\sigma_{rR_{\mathrm{p}}}$ represents the radial stress at the junction of the elastic zone of the surrounding rock and the unanchored elastic zone.

The surrounding rock stresses and radial displacements in the anchored plastic zone are similar to Eqs. (19) and (21) which can be expressed as

$$u^{\mathrm{p3}}\left(r,X\right)=r^{-\eta_3}\left(R_{\mathrm{p}}^{\eta_3}u^{\mathrm{e1}}\left(R_{\mathrm{p}},X\right)-\frac{\left(1+\mu\right)\left[\lambda\left(X\right)p_0-\sigma_{rR_{\mathrm{p}}}\right]\left(\eta_3-1\right)}{E}\left(R_{\mathrm{p}}^{1+\eta_3}-r^{1+\eta_3}\right)\right)\tag{25}$$

where $H_7=\left.\dfrac{\partial u^{\mathrm{p3}}\left(r,X\right)}{\partial r}\right|_{r=L_0}+\eta_2\left.\dfrac{u^{\mathrm{p3}}\left(r,X\right)}{r}\right|_{r=L_0}$.

At this point, the surrounding rock stresses and radial displacements in the anchored plastic reinforcement zone are consistent with Eq. (22)

3.4 Plastic zone radius solution

Since the radius R_{p} of the plastic zone is unknown, it is not possible to directly derive the surrounding rock stresses and displacements. Since the radial stresses at the cave wall are equal in magnitude to the supporting pressure of the lining, there is

$$p_1=\sigma_r^{\mathrm{p1}}\left(r_0,X\right)=K_1u^{\mathrm{p1}}\left(r_0,X\right)\tag{26}$$

where K_1 is the primary support stiffness (excluding rockbolts, which are considered as composite bearers in combination with the surrounding rock). In weak rock tunnels, shotcrete and steel arches should be included, and the expression for the stiffness of these two materials can be written as (Oreste 2003)

$$\begin{cases}K_{11}=\dfrac{E_{\mathrm{c}}\left(r_0^2-r_1^2\right)}{\left(1+\mu_{\mathrm{c}}\right)\left[\left(1-2\mu_{\mathrm{c}}\right)r_0^2+r_1^2\right]}\dfrac{1}{r_0}\\ K_{12}=\dfrac{E_{\mathrm{st}}A_{\mathrm{set}}}{S\left(r_0-h_{\mathrm{set}}/2\right)^2}\end{cases}\tag{27}$$

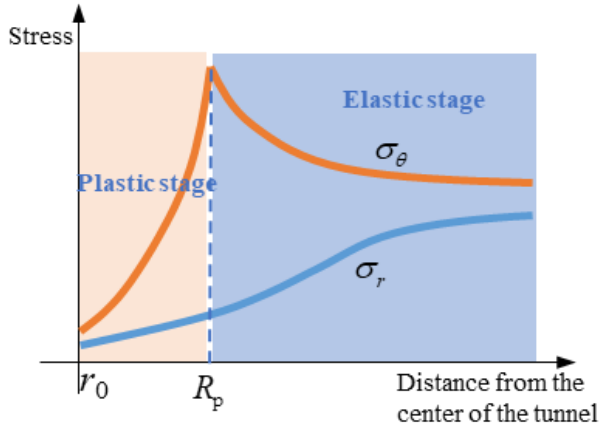

Fig. 3 Schematic diagram of surrounding rock stresses

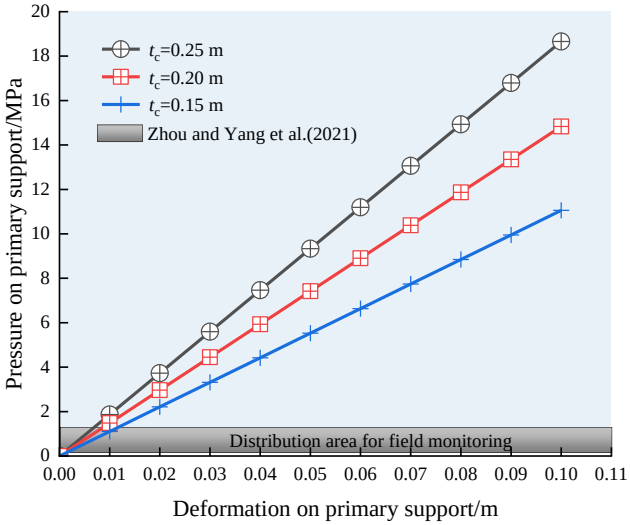

Fig. 4 Variation of tunnel support pressure with deformation

where E_c and r_1 are the elastic modulus and internal diameter of shotcrete, respectively. μ_c is the Poisson's ratio of the shotcrete. E_{st}, A_{set}, S and h_{set} are the elastic modulus, cross-sectional area, layout spacing and section height of the steel arch, respectively.

Thus, the radius of the plastic zone R_p can be found by using Eq. (26) and combining it with the previous relevant derivation.

3.5 Discussion of support pressure calculations

In the past, the active setting of the support pressure was used, which led to the radius calculation of the plastic zone being larger than the actual one. In fact, the support pressure is the result of the interaction between the surrounding rock and the support structure. Eq. (26) must reasonably determine the magnitude of the support pressure (contact pressure between the surrounding rock and the primary support). According to the previous stress curve distribution diagram in the surrounding rock (Fig. 3, Xu *et al.* 2021, Sheng *et al.* 2023), the support pressure at the cave wall should be the minimum. However, the support pressure calculated by Eq. (26) is surprisingly large, even larger than the tangential stress in the surrounding rock. It is assumed that the elastic modulus and Poisson's ratio of the primary support are 25 GPa and 0.2 respectively, and the radius of the tunnel is 6 m. The load sharing of the initial support with different thicknesses of shotcrete calculated according to Eq. (26) can be presented in Fig. 4. It is not difficult to find that the load of the primary support is very much affected by the deformation on the primary support, and the load increases by about 1.8 MPa for every 1 cm increase in deformation. According to Zhou and Yang (2021) on the load on the primary support of the field monitoring study, the load shared by the primary support of Class V surrounding rock is generally within 1 MPa, up to 1.5 MPa, and the load shared by the primary support of medium surrounding rock is not even more than 0.15 MPa, which fully demonstrates that the existing method of calculating the pressure of the support is in need of urgent revision.

4. Correction of the calculation method of support pressure

Active support embodies a rigid support concept that cannot meet the current status of shotcrete-bolt flexible support as specified in the code. This is also the reason for the current large error in the calculation of traditional support pressure. The primary support moves as the surrounding rock moves closer to the cave. It is generally ductile enough not to break within the allowable deformation. Surrounding rock load is released during the process of "resisting and yielding" of the primary support, and the pressure of the surrounding rock also increases with the increase of the deformation of the surrounding rock, as described in Fig. 5.

The main reason for the exaggerated support pressures is that the rigid support philosophy creates an inevitable relationship between support pressures and the deformation of the surrounding rock. Every 1 mm of surrounding rock deformation generates a larger support pressure after the support structure is installed. In fact, according to Newton's second law, the force on an object is related to its acceleration, i.e., the force between objects increases, remains unchanged and decreases when the object is in accelerated, uniform or decelerated motion. Thus, the support pressure is not generated as long as the deformation is generated after the support installation, but the support pressure is related to the movement state of the surrounding rock in the interaction with the support structure. That is to say, the surrounding rock has generated virtual support pressure before the primary support is installed. This virtual support pressure is different from the previous virtual support force, which is the load of the surrounding rock in the excavation process. The virtual support pressure in this study is the force on the surrounding rock along the tunnel profile in front of the excavation advancement to the primary support installation, which can be list schematically in Fig. 6.

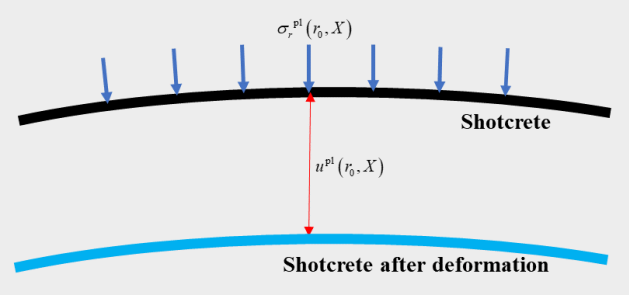

Fig. 5 Variation of tunnel support pressure with deformation

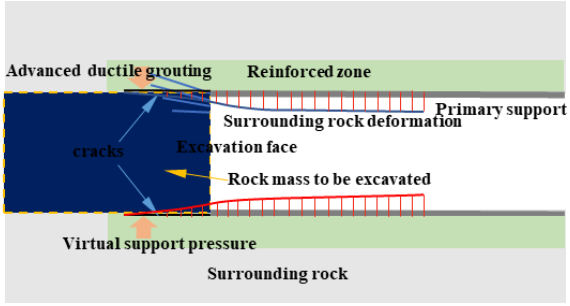

Fig. 6 Displacement and loading diagram in front and behind the tunnel excavation face

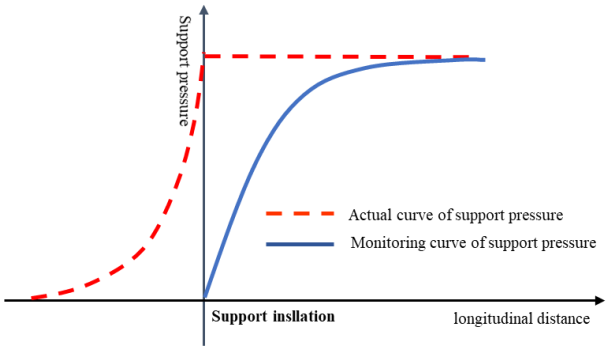

Fig. 7 Comparison between the actual paths of surrounding rock and support pressure and field measurements

A large amount of monitoring data reveals that change in support pressure observed during field monitoring does not follow a consistent pattern. The pressure initially starts increasing from 0 and eventually stabilizes, which is not in line with the expected change in support pressure. However, the study argues that this discrepancy is due to a hysteresis effect on the contact pressure that is monitored in the field. The pressure recorded by the pressure box gradually increases from 0 to the load at which the primary support was first installed. This increase does not happen abruptly, but rather occurs over a period of time. Despite the differences between the support pressures observed in the field and the expected development path, the final support pressure values converge. Based on the comparison between the actual path of the support pressure and the field measurements, the study presents a new concept for predicting tunnel support pressure. It explains that the generation of support pressure is influenced by the

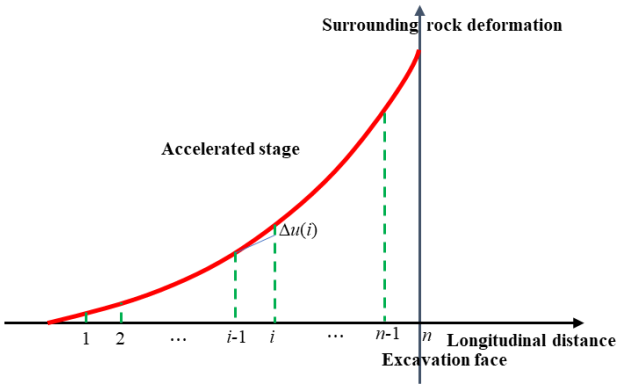

Fig. 8 Comparison between the actual path of support pressure and field measurements

movement of the surrounding rock rather than the deformation of the rock itself. Fig. 7 illustrates the results of this comparison.

Since the reduction magnitude is small and difficult to determine, it can be considered negligible in the estimation of support pressure reduction. Support pressure consists of two stages: increasing and constant. Currently, the calculation of support pressure is based on Eq. (26). However, in order to consider the flexibility of the support, this study must take into account the deformation of surrounding rock in relation to support pressure. Thus, only the deformation generated during accelerated motion of the surrounding rock minus the deformation generated at a constant speed is considered as the contact load between the surrounding rock and the primary support. The calculation of support pressure during accelerated motion of the surrounding rock can be based on the calculation shown in Fig. 8.

In Fig. 8, the surrounding rock is divided into n segments for accelerated movement stage, and the general pre-deformation range is generally $3\,r_0 / n$ in front of the excavation face, then the length of each segment of weak surrounding rock is $3\,r_0 / n$. The displacement increment related to the support pressure for the ith segment is $\Delta u(i)$, which can be obtained by subtracting the actual deformation at the end of the ith segment from that at the end of the i-1th segment due to the uniform movement of the surrounding rock. The deformation of the surrounding rock during the accelerated motion stage has the following equation.

$$u^{p2}(r_0, X) = r_0^{-\eta_2}\left(L_0^{\eta_2} u^{p3}(L_0, X) - \frac{H_7}{1+\eta_2} L_0^{1+\eta_2} + \frac{H_7}{1+\eta_2} r_0^{1+\eta_2}\right) \quad (28)$$

The slope of the pre-deformation of the surrounding rock can be obtained by taking the first order derivative of X in $u^{p2}(r, X)$, which can be written as

$$u^{p2}(r_0, X) = r_0^{-\eta_2}\left(L_0^{\eta_2} u^{p3}(L_0, X) - \frac{H_7}{1+\eta_2} L_0^{1+\eta_2} + \frac{H_7}{1+\eta_2} r_0^{1+\eta_2}\right) \quad (29)$$

Next, the i-1th segment end tangent equation should be required. The coordinate of the point on the i-1th segment end displacement curve can be calculated as

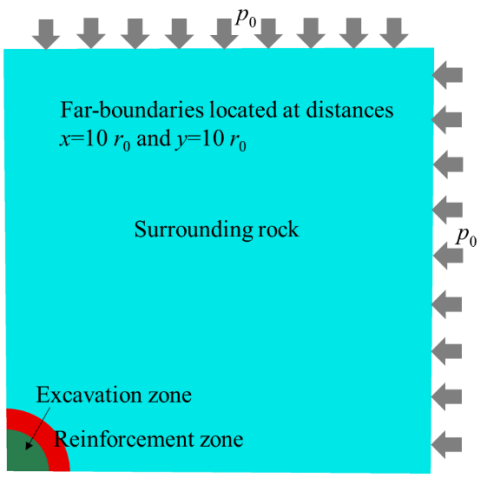

Fig. 9 3D model of the tunnel

$\left(-3r_0\dfrac{n+1-i}{n}, u\left(r_0, -3r_0\dfrac{n+1-i}{n}\right)\right)$, and the i-1th segment end tangent equation can be written as

$$u_{i-1}^{p2}(r_0, X) = r_0^{-\eta_2}\left(L_0^{\eta_2}\frac{\partial u^{p3}(L_0, X)}{\partial X} - \frac{H_7}{1+\eta_2}L_0^{1+\eta_2} + \frac{H_7}{1+\eta_2}r_0^{1+\eta_2}\right)\left(X + 3r_0\frac{n+1-i}{n}\right) + u\left(r_0, -1.5r_0\frac{n+1-i}{n}\right) \quad (30)$$

At this point, the value at the end of segment i can be expressed as

$$u_i^{p2}\left(r_0, -3r_0\frac{n-i}{n}\right) = r_0^{-\eta_2}\left(L_0^{\eta_2}\frac{\partial u^{p3}\left(L_0, -3r_0\frac{n-i}{n}\right)}{\partial X} - \frac{H_7}{1+\eta_2}L_0^{1+\eta_2} + \frac{H_7}{1+\eta_2}r_0^{1+\eta_2}\right)\frac{3r_0}{n} + u\left(r_0, -1.5r_0\frac{n+1-i}{n}\right) \quad (31)$$

Then, the displacement increment $\Delta u(i)$ associated with shotcrete loading in section i can be written as

$$\Delta u(i) = u_i^{p2}\left(r_0, -3r_0\frac{n-i}{n}\right) - u_{i-1}^{p2}\left(r_0, -3r_0\frac{n-i}{n}\right) \quad (32)$$

The formula for calculating the support pressure during the pre-deformation stage can be rewritten as follows.

$$p_1(X=0) = \sum_{i=1}^{n}(K_1 + K_{12})\Delta u(i) \quad (33)$$

5. Numerical simulation validation of the theoretical approach

To validate the theoretical analysis, a 3D simulation of the construction process of a deep-buried tunnel was conducted using FLAC3D6.0 software. The tunnel section was circular with a radius of 6 m. To minimize boundary effects, the model size was set to 60 m × 60 m × 60 m, with a boundary length more than 5 times the diameter of the tunnel. Due to the tunnel's symmetry, only 1/4 of the model was studied. Fig. 9 shows the plan view of the constructed model.Fixed constraints were applied to the front, back, left, and lower sides of the model, while the other faces were considered free ends with uniform loads. The in-situ stress was set to 6 MPa. The self-weight of the surrounding rock and support structure was not considered. Excavation was carried out in increments of 3 m, with a pre-reinforcement zone and primary support implemented after each excavation face. To simulate the support structure, Shell units were used to represent shotcrete, while Beam units were used to simulate steel arches and rockbolts. The monitoring section was selected in the middle of the tunnel excavation direction.

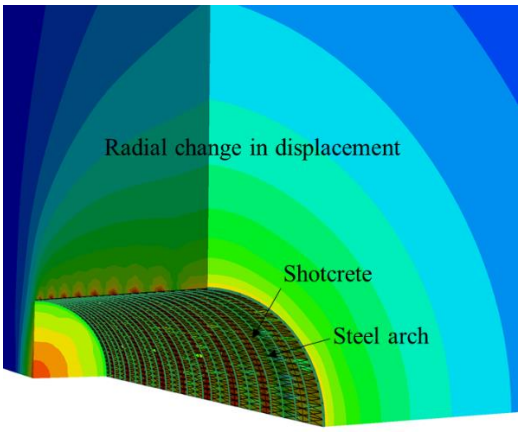

Fig. 10 Tunnel displacement cloud

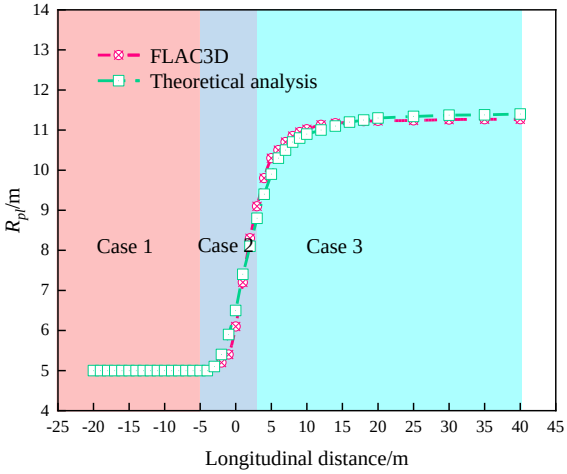

Fig. 11 Comparison of theoretical solution and numerically calculated plastic zone radius evolution paths

The Mohr-Coulomb criterion was proposed to be used for the constitutive model of the surrounding rock. The basic design parameters of the surrounding rock can be list in Table 1. In addition, the Poisson's ratio of the anchored plastic zone and the anchored pre-reinforcement zone is also 0.25.

The support parameters of the tunnel were designed as list in Table 2. The displacement cloud diagram during tunnel excavation can be indicated in Fig. 10.

In Fig. 11, a comparison is presented between the solution obtained in this study and the results of a numerical simulation, regarding the evolution of the radius of the plastic zone in the surrounding rock. Although there are slight differences in the development process of the two plastic zones, they follow a similar trend. This indicates that the theoretical calculation is in an agreement with the evolution trend of the plastic zone in the surrounding rock. Furthermore, the final radius of the plastic zone obtained

Table 1 Basic design parameters of surrounding rock

Parameters	Surrounding rock				Pre-reinforcement zone			
	Cohesion /MPa	Internal friction angle /°	Elastic modulus /GPa	Poisson's ratio	Cohesion /MPa	Internal friction angle /°	Elastic modulus /GPa	Poisson's ratio
Value	2	30	1	0.25	4	30	2	0.25

Table 2 Basic design parameters of surrounding rock

Support structure	Parameters	Value
Shotcrete	Elastic modulus /GPa	25
	Poisson's ratio	0.2
	Thickness /m	0.25
Rockbolt	Elastic modulus /GPa	200
	Length /m	3
	Spacing and row spacing /m	1
	Diameter /m	0.042
Steel arch	Elastic modulus /GPa	206
	Cross-sectional area /cm^2	39.578
	Section height /mm	200
	Spacing /m	0.9

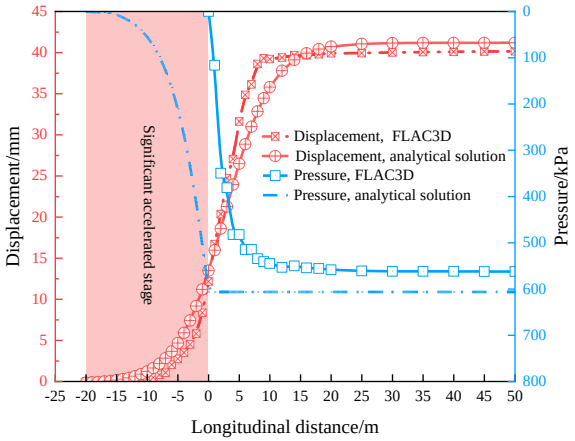

Fig. 12 Comparison of theoretical solution and numerical calculation of surrounding rock displacement and support pressure

from the theoretical calculation is 11.42 m, while the numerical simulation yields a radius of 11.24 m. The difference between the two values is only about 1.6%. This small discrepancy suggests that the two calculation methods are essentially consistent in predicting the radius of the plastic zone. Therefore, the theory proposed in this paper is considered feasible in describing the evolution of the plastic zone in the surrounding rock.

The comparative analysis of surrounding rock deformation and support pressure between the solution proposed in this study and numerical simulation can be seen in Fig. 12. Although the two methods demonstrate different evolution patterns of surrounding rock deformation, they both exhibit the same overall trend. The theoretical solution predicts a surrounding rock deformation of 41.20 mm, while the numerical simulation predicts a deformation of 41.17 mm, resulting in an error of only 2.5%. The development path of the support pressure shows some differences, but it aligns with the assumption made in Section IV and demonstrates the expected evolution pattern. The final support pressure values are quite similar, with values of 606.4 kPa and 562.3 kPa respectively. The error between the two is 7.8%, which is significantly smaller than the calculation errors typically observed in traditional methods, which can be several times or even an order of magnitude higher. Thus, the results of this study closely align with the numerical simulation, confirming the accuracy of the theoretical method proposed in this paper in predicting the plastic zone radius of the surrounding rock, the deformation of the surrounding rock, and the support pressure.

6. Parametric analysis of analytical solutions for deep-buried tunnels

The parameter analysis mainly reflects the change of one or two parameters to reflect the change of surrounding rock stress, deformation and support pressure. Thus, the parameters of this study are still mainly listed in the previous section. The parameter analysis is mainly divided into three parts to study the effects of different parameters on the surrounding rock parameters, surrounding rock deformation and support pressure. The following is the related analysis.

6.1 Effect of different parameters on the internal parameters of the surrounding rock

Fig. 13 illustrates the impact of cohesion on radial and

tangential stresses in the surrounding rock of the pre-reinforcement zone. It is obvious to see that the radial and tangential stresses in the anchored pre-consolidation zone of the surrounding rock increase with r. In contrast, the unanchored plastic zone exhibits a dramatic increase in stress, with the tangential stress exceeding the radial stress. In the elastic zone of the surrounding rock, the tangential stress gradually decreases, while the increase in radial stress tends to stabilize at a slower rate. Increasing the cohesion by 1 MPa in the anchored pre-reinforcement zone results in a decrease of approximately 0.8 MPa in both tangential and radial stresses at infinity from the hole center. Additionally, the tangential stress at the elastoplastic junction decreases by approximately 1.2 MPa. The thickness of the pre-reinforcement zone, defined as b, plays a role in these stress changes. Fig. 14 supports the finding that for every 1 MPa increase in cohesion in the anchored pre-reinforcement zone, the tangential and radial stresses at an infinite distance from the hole center decrease by approximately 0.9 MPa and 0.6 MPa, respectively. Moreover, the tangential stress at the elastoplastic junction decreases by about 1.2 MPa, and the plastic zone's radius decreases by roughly 1 m. These findings demonstrate that increasing the thickness of the pre-reinforced zone leads to a decrease in peak stress and a narrowing of the plastic zone. However, it is important to note that this comes at a significantly higher cost for the pre-reinforcement zone.Fig. 15 shows the effect of in-situ stress p_0 and support pressure p_i on the radius of the plastic zone of the surrounding rock. For a certain value of one of the parameters of in-situ stress and support pressure, the larger the value of the other parameter, the radius of the plastic zone shows a tendency to decrease. All the surrounding rocks will produce unanchored plastic zones when p_0 is greater than 6 MPa. When p_0 is equal to 2 MPa and p_i is less than 0.5 MPa, the plastic zone is located in the unanchored plastic zone. When p_i is greater than 0.5 MPa and less than 1.1 MPa, the plastic zone is located in the anchored pre-reinforcement zone. The surrounding rock does not produce a plastic zone if the p_i is greater than 1.1 MPa. Fig. 16 depicts how the internal strain of the surrounding rock is influenced by in-situ stress. Within the anchored pre-reinforcement zone, the strain in the surrounding rock decreases rapidly, with the tangential strain decreasing more than the radial strain. As the rock enters the elastic zone, the rate of strain reduction slows down, eventually stabilizing, indicating minimal deformation in the elastic zone. An increase of 2 MPa in in-situ stress results in approximately a 1.6×10^{-3} increase in maximum radial strain and a 4.6×10^{-3} increase in maximum tangential strain in the surrounding rock.

The parameters in the pre-reinforcement zone play a significant role in the variation of stress within the surrounding rock. Additionally, the in-situ stress has a notable impact on the radius of the plastic zone in the surrounding rock and its strain within the pre-reinforcement zone. Hence, optimizing the parameters in the pre-reinforcement zone can effectively reduce deformation and the radius of the plastic zone in weak surrounding rock for deep-buried tunnels.

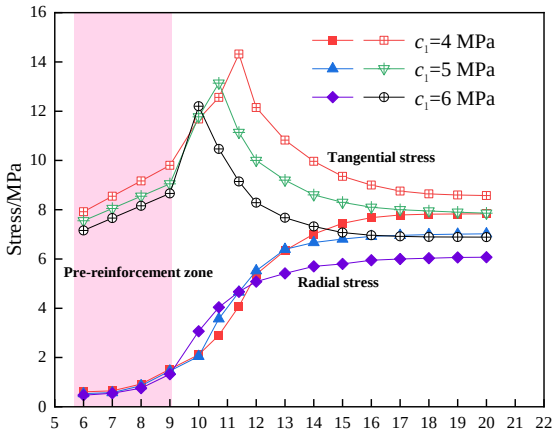

Fig. 13 Effect of cohesion on surrounding rock stresses in the anchored pre-reinforcement zone

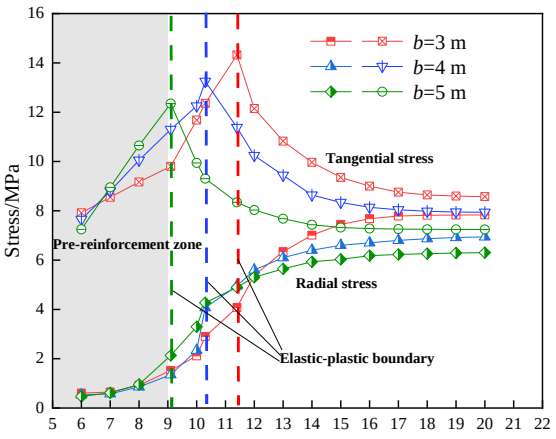

Fig. 14 Effect of the thickness of the anchored pre-reinforcement zone on the stresses in the surrounding rock

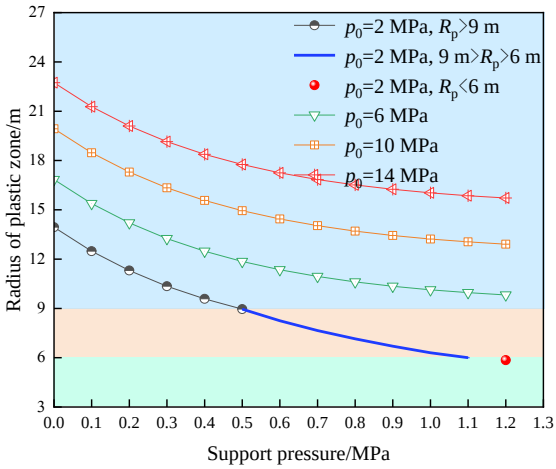

Fig. 15 Effect of in-situ stress and support pressure on the plastic zone of the surrounding rock

6.2 Effect of different parameters on the deformation of the surrounding rock

The effects of different factors on surrounding rock

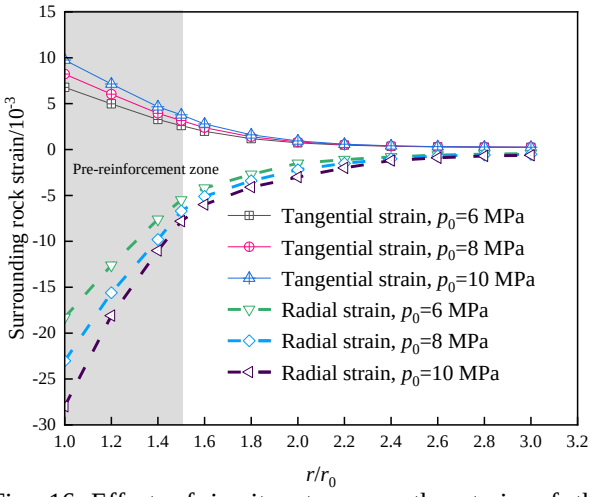

Fig. 16 Effect of in-situ stress on the strain of the surrounding rock

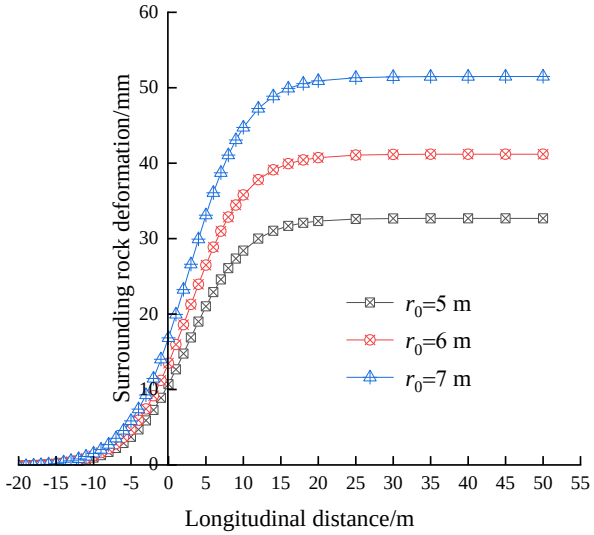

Fig. 17 Effect of r_0 on the deformation of the surrounding rock

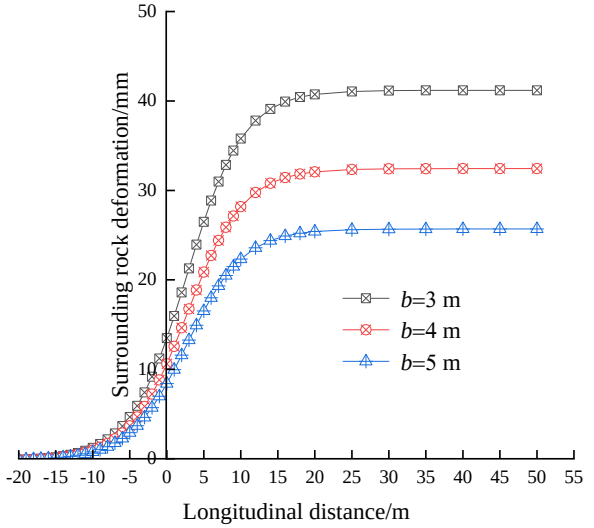

Fig. 18 Effect of b on the deformation of the surrounding rock

deformation were analyzed and depicted in Figs. 17 to 20. Fig. 17 demonstrates that the deformation of the surrounding rock and the excavation distance of the tunnel experience an acceleration phase, followed by a uniform speed phase, a deceleration phase, and finally reaching a stabilization state. This finding aligns with the previous conception of this study. Moreover, it was observed that the deformation of the surrounding rock at the excavation face and end increases with an increase in tunnel radius. Specifically, for each meter increase in the tunnel radius, the final deformation of the surrounding rock increases by approximately 10 mm. This effect is particularly noticeable. Fig. 18 examines the impact of the thickness b of the pre-reinforcement zone on the surrounding rock deformation. The trend of the surrounding rock deformation is similar to that of the tunnel radius. For each meter increase in the thickness b of the pre-reinforcement zone, the final deformation of the surrounding rock decreases by about 9 mm. This finding indicates that increasing the thickness of the pre-reinforcement zone can effectively reduce the deformation of the surrounding rock. Fig. 19 illustrates the impact of the elastic modulus of shotcrete on support pressure. It demonstrates that, irrespective of the elastic modulus of the shotcrete, the path of surrounding rock deformation change is consistent in front of the excavation face. However, behind the excavation face, a higher elastic modulus results in a smaller surrounding rock deformation. This relationship between the elastic modulus and surrounding rock deformation is notable, with a 6 mm reduction in deformation observed for every 5 GPa increase in the elastic modulus of the shotcrete. This finding indicates that enhancing the strength of the support effectively reduces the deformation of the surrounding rock.In Fig. 20, we observe the effect of support time on the deformation of the surrounding rock. It is clear that the support time has a more significant influence on the surrounding rock deformation. Specifically, in front of the excavation surface, the support timing has no impact on the deformation of the surrounding rock. However, behind the excavation face, delaying the installation of support by 3 meters increases the deformation of the surrounding rock by approximately 10 mm. This emphasizes the importance of promptly installing support in areas with weak surrounding rock at depth.

In summary, the material parameters of the pre-reinforcement zone affect the surrounding rock deformation during the whole process, while the support material parameters and the support time mainly affect the surrounding rock deformation behind the excavation face. Pre-reinforcement suppresses the surrounding rock deformation obviously, but the construction cost must be considered. It is recommended that the deep-buried surrounding rock section prone to instability should be grouted in advance to reinforce the surrounding rock in front of the excavation face, and the support should closely follow the excavation face. Moreover, the stiffness of shotcrete can be improved to suppress the deformation of surrounding rock if the cost is allowed.

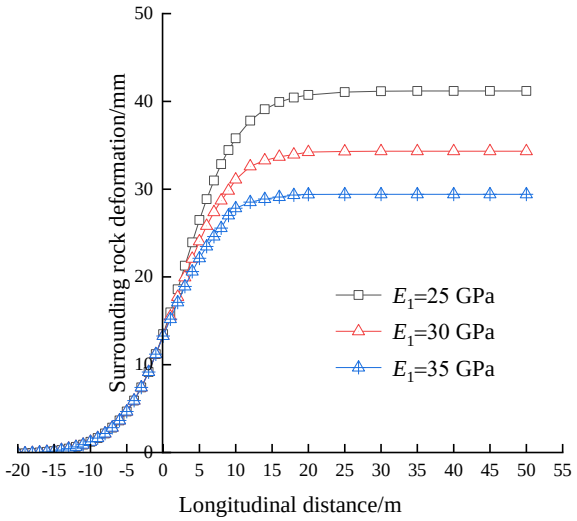

Fig. 19 Effect of E_1 on the deformation of the surrounding rock

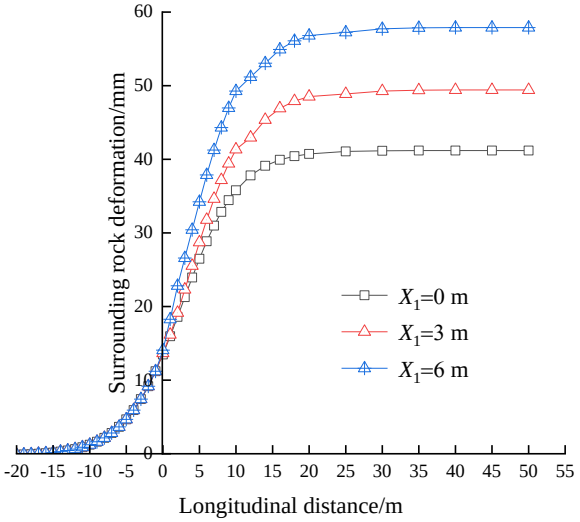

Fig. 20 Effect of support time on the deformation of the surrounding rock

In conclusion, the material parameters of the pre-reinforcement zone have a significant impact on the deformation of the surrounding rock throughout the entire process, while the support material parameters and support time primarily affect the deformation behind the excavation face. Pre-reinforcement effectively reduces the deformation of the surrounding rock. However, it is crucial to consider the construction cost. It is therefore recommended to grout the deep-buried unstable surrounding rock section in advance to reinforce the area in front of the excavation face, and ensure that the support closely follows the excavation. Additionally, if cost permits, improving the stiffness of the shotcrete can further help in suppressing the deformation of the surrounding rock.

6.3 Effect of different parameters on support pressure

Figs. 21 to 25 depict the impact of various factors on support pressure in a tunnel. Fig. 21 demonstrates that support pressure increases in a non-linear manner ahead of the excavation face but remains constant behind it. For each additional meter of tunnel radius r_0, the support pressure rises by more than 140 kPa, which indicates a significant effect. Fig. 22 highlights the correlation between in-situ stress and support pressure, whereby a 2 MPa increase in p_0 results in approximately 110 kPa increase in support pressure. The influence of cohesion in the pre-reinforcement zone on support pressure is illustrated in Fig. 23. It is evident that this factor has less significance compared to tunnel radius and in-situ stress. This can be attributed to the limited acceleration of deformation in the surrounding rock, as the support pressure is associated with this deformation.

Figs. 21 to 25 show the effect of tunnel radius, in-situ stress, cohesion in the pre-reinforcement zone, displacement release coefficient and elastic modulus of shotcrete on the support pressure. According to Fig. 21, the support pressure increases non-linearly in front of the excavation face and remains constant behind the excavation face. For every 1 meter increase in the tunnel radius r_0, the support pressure increases by more than 140 kPa, which is a more significant effect. It is easy to elaborate from Fig. 22 that the effect of in-situ stress p_0 on the support pressure is more consistent with r_0. For every 2 MPa increase in p_0, the support pressure increases by about 110 kPa. Fig. 23 shows the effect of cohesion in the pre-reinforcement zone on the support pressure. It is obvious to find that the effect of cohesion in the pre-reinforcement zone on the support pressure is not as significant as that of the tunnel radius and the in-situ stress, which is due to the accelerated deformation of the surrounding rock associated with the support pressure, while the true accelerated deformation of the surrounding rock has limited values. Fig. 24 presents the effect of displacement release coefficient on the support pressure. In the figure, u_0 and u_∞ represent the surrounding rock displacements at the tunnel excavation face and the final surrounding rock displacements, respectively. If the total surrounding rock deformation is determined, the larger the displacement release rate is, the larger the support pressure can be shared. For every 0.1 increase in the displacement release coefficient, the pressure shared by the support increases by about 200 kPa, which is a significant effect. From Fig. 25, it is easy to see that the support pressure increases gradually with the increase the thickness or elastic modulus of shotcrete. For every 5 GPa increase in the elastic modulus of shotcrete, the support pressure increases by about 120 kPa. It is the deformation of the surrounding rock in front of the excavation cannot change due to changes in the support parameters, then the support pressure depends on the support stiffness.

Overall, R_0, p_0 and the displacement release coefficient share more pressure on the support. However, R_0 and p_0 are generally decided according to the tunnel design needs and the ground environment, which generally cannot be changed. The reduction of the advanced displacement is decisive for the eventual reduction of the support pressure

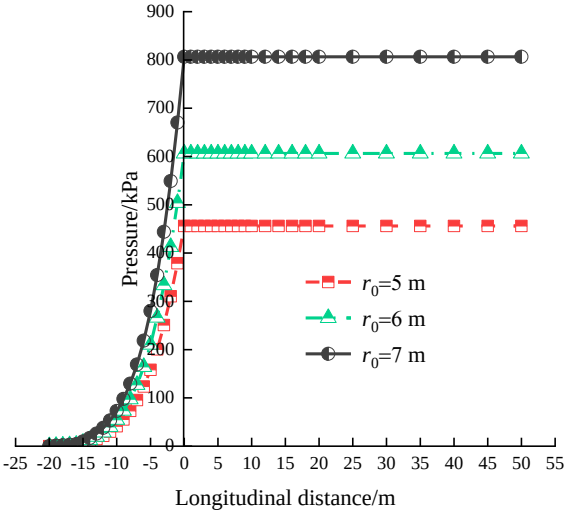

Fig. 21 The effect of r_0 on support pressure

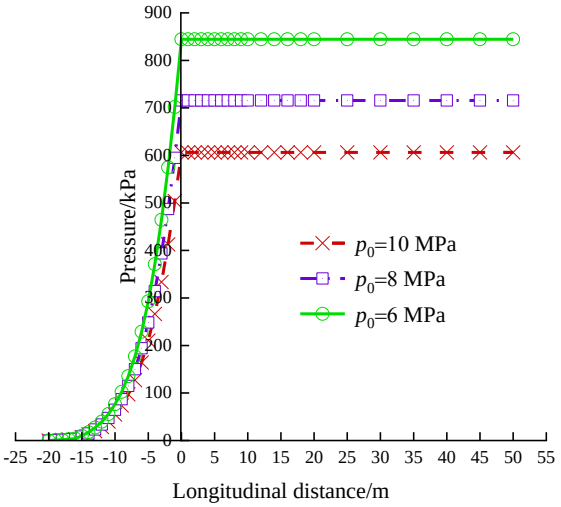

Fig. 22 The effect of p_0 on support pressure

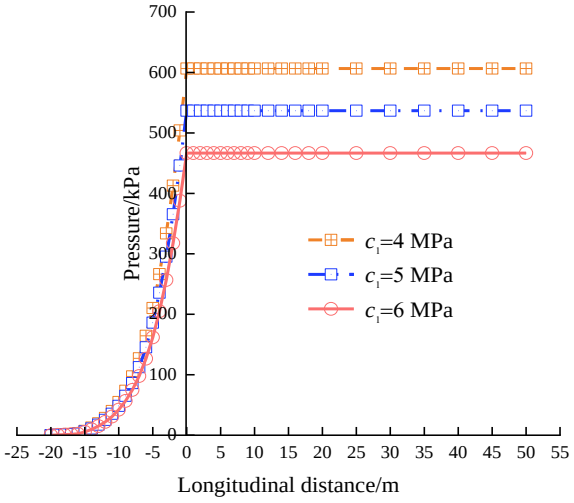

Fig. 23 The effect of c_1 on support pressure

only by reducing the rate of deformation of the surrounding rock in front of the excavation. Moreover, the increase in the strength of the surrounding rock pre-reinforcement zone

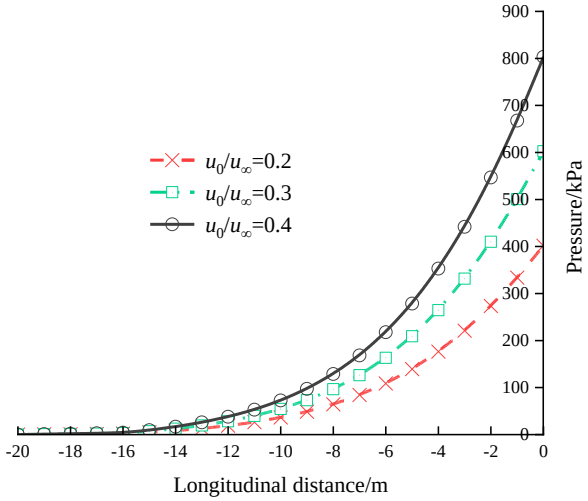

Fig. 24 The effect of u_0/u_∞ on support pressure

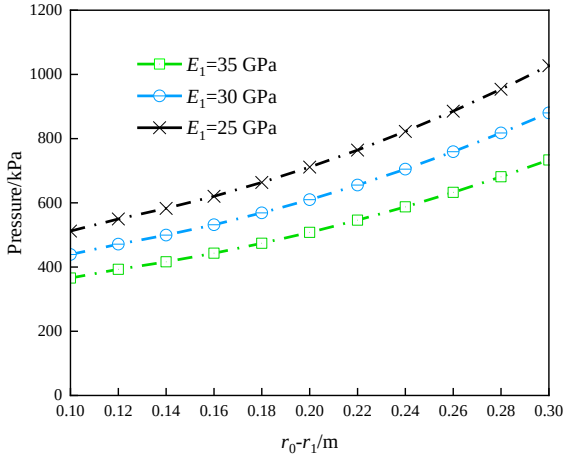

Fig. 25 Elastic modulus effect of shotcrete on support pressure

and the increase in the strength of the shotcrete have opposite effects on the support pressure, mainly because the surrounding rock pre-reinforcement zone inhibits the advanced deformation of the surrounding rock, whereas the strength of the shotcrete is only related to the deformation of the support after the installation of the support. Thus, for the weak surrounding rock, the pre-support can be strengthened to reduce the pre-deformation of the surrounding rock, thus reducing the final support pressure. The stiffness of the support can be reduced if the conditions for controlling the deformation of the surrounding rock allow it, thus saving costs and reducing the support pressure.

7. Conclusions

In this study, it has developed a comprehensive model to accurately depict the evolution process of tunnels with pre-reinforcement rock mass. The underlying interaction mechanism between flexible support and surrounding rock was uncovered, thereby rectifying the inaccuracies in the previous analytical solution for 3D tunnel construction. By

conducting numerical simulations, the several innovative findings that validate the effectiveness of our proposed procedure were obtained.

(1) The parameters of the pre-reinforcement zone in the surrounding rock had a significant effect on the stress in the surrounding rock. The primary function of the pre-reinforcement zone was to suppress pre-deformation in the surrounding rock, thereby reducing support pressure. It is recommended to design the parameters of the pre-reinforcement zone while considering the affordable construction cost and ensuring construction safety.

(2) The kinematics of the surrounding rock was taken into account to analyze the variation in support pressure over time. The pressure exerted on the support system during the acceleration, uniform velocity, and deceleration phases of the surrounding rock exhibited an increasing, constant, and decreasing trend, respectively. In this study, we simplified the existence of accelerating and uniform velocity stages in the behavior of the surrounding rock. The development of support pressure was found to be highly influenced by the deformation of the surrounding rock during the accelerated movement in the advanced stage of tunnel construction.

(3) The sections of surrounding rock deep underground, which are susceptible to instability, were extensively treated with advanced grouting methods to strengthen the rock surrounding the excavation. The support system closely follows the excavation face. Moreover, when cost allows, the stiffness of the shotcrete can be enhanced to restrict the deformation of the surrounding rock, thereby limiting the increase in support pressure on the rock. This approach has a significant impact on ensuring the safety of weak surrounding rock tunnel construction.

(4) The correctness of the analytical solution was verified by comparing and analyzing the analytical solution and numerical simulation results in this study. The error in the radius of plastic zone between analytical solution and numerical simulation is about 1.6%, the error in the deformation of surrounding rock is not more than 2.5%, and the error in the load shared by the primary support is not more than 7.8%. The comparative results show a good agreement.

(5) The determination of factors R_0 and p_0 is typically based on the specific requirements of the tunnel design and the characteristics of the ground environment. However, the key factor in reducing the support pressure is minimizing the rate of deformation of the surrounding rock ahead of the excavation, which directly influences the advancement displacement. Importantly, the strength of the pre-reinforcement zone and shotcrete have contrasting effects on the support pressure. Increasing the strength of the pre-reinforcement zone and shotcrete will have an opposite effect on the support pressure. Hence, it is crucial to optimize the parameters of the pre-reinforcement zone and support material to strike a balance between minimizing surrounding rock deformation, managing support pressure, cost considerations, and ensuring safety.

(6) Pre-reinforcement in rock mass can effectively reduce the deformation of the tunnel surrounding rock and the load shared by the primary support, and the consolidation effect is obvious. This technology can be used in combination with the cost of support in the deep-buried weak surrounding rock with large deformation section to ensure the safety of tunnel boring.

Acknowledgements

This study is sponsored by the Scientific Research Project of Zhejiang Provincial Department of Education (Y202351526) and Scientific Research Project of Zhejiang Provincial Transportation Department (2021050). The financial supports are greatly appreciated.

References

Bian, Y., Xia, C., Xiao, W. and Zhang, G. (2013), "Visco-elastoplastic solutions for circular tunnel considering stress release and softening behaviour of rocks", *Rock. Soil Mech.*, **1**, 211-220.

Carranza-Torres, C., Rysdahl, B. and Kasim, M. (2013), "On the elastic analysis of a circular lined tunnel considering the delayed installation of the support", *Int. J. Rock. Mech. Min. Sci.*, **61**, 57-85. https://doi.org/10.1016/j.ijrmms.2013.01.010.

Cheng, K., Xu, R.Q., Ying, H.W., Lin, C.A., Gan, X.L., Gong, X.A., Zhu, J.F. and Liu, S.J. (2023), "Analytical method for predicting tunnel heave due to overlying excavation considering spatial effect", *Tunn. Undergr. Sp.. Technol.*, **138**, 105169. https://doi.org/10.1016/j.tust.2023.105169.

Chu, Z.F., Wu, Z.J., Liu, Q.S., Weng, L., Xu, X.Y., Wu, K. and Sun, Z.Y. (2024), "Viscos-elastic-plastic solution for deep buried tunnels considering tunnel face effect and sequential installation of double linings", *Comput. Geotech.*, **165**, 105930. https://doi.org/10.1016/j.compgeo.2023.105930.

Cui, L., Zheng, J.J., Zhang, R. and Lai, H.J. (2015), "A numerical procedure for the fictitious support pressure in the application of the convergence–confinement method for circular tunnel design", *Int. J. Rock. Mech. Min. Sci.*, **78**, 336-349. https://doi.org/10.1016/j.ijrmms.2015.07.001.

Dehghan, A.N., Shafiee, S.M. and Rezaei, F. (2012), "3-D stability analysis and design of the primary support of Karaj metro Tunnel: Based on convergence data and back analysis algorithm", *Eng. Geol.* **141**, 141–149. https://doi.org/10.1016/j.enggeo.2012.05.008.

Ghorbani, A., Hasanzadehshooiili, H. and Sadowski, L. (2018), "Neural prediction of tunnels' support pressure in elasto-plastic, strain-softening rock mass", *Appl. Sci.*, **8**, 441. https://doi.org/10.3390/app8050841.

Iasiello, C., Torralbo, J.C.G. and Fernández, C.T. (2021), "Large deformations in deep tunnels excavated in weak rocks: Study on Y-Basque high-speed railway tunnels in northern Spain", *Undergr. Sp.*, **6**, 636–649. https://doi.org/10.1016/j.undsp.2021.02.001.

Indraratna, B. and Kaiser, P.K. (1990), "Analytical model for the design of grouted rock bolts", *Int. J. Num. Anal. Meth. Geomech.*, **14**, 227–251. https://doi.org/10.1002/nag.1610140402.

Lee, Y.L., Hsu, W.K., Lee, C.M., Xin, Y.X. and Zhou, B.Y. (2020), "Direct calculation method for the analysis of non-linear behavior of ground-support interaction of a circular tunnel using convergence confinement approach", *Geotech. Geol. Eng.*, **39**, 973–990. https://doi.org/10.1007/s10706-020-01539-4.

Li, P.F., Cui, X.P., Xia, J.W. and Wang, X.Y. (2023), "Analytical solutions of limit support pressure and vertical earth pressure on cutting face for tunnels", *Undergr. Sp.*, **12**, 51-69. https://doi.org/10.1016/j.undsp.2023.02.004.

Mirzaeiabdolyousefi, M., Nikkhah, M. and Zare, S. (2022), "Assessment of time-dependent behaviour of rocks on concrete lining in a large cross-section tunnel", *Geomech. Eng.*, **29**(1), 41-51. https://doi.org/10.12989/gae.2022.29.1.041.

Osgoui, R.R. (2006), "Ground reaction curve of reinforced tunnel using a new elasto-plastic model", Turin, The Technical University of Turin.

Oreste, P.P. (2003), "Analysis of structural interaction in tunnels using the convergence–conffnement approach", *Tunn. Undergr. Space. Technol.* **18**, 347–363.

Panthi, K.K., Shrestha, P.K. (2018), "Estimating tunnel strain in the weak and schistose rock mass influenced by stress anisotropy: an evaluation based on three tunnel cases from Nepal", *Rock. Mech. Rock. Eng.*, **51**(6), 1823-1838. https://doi.org/10.1007/s00603-018-1448-7.

Pandit, B. and Babu, G.L.S. (2022), "Global sensitivity analysis for a tunnel-support system in weak rock mass for both-uncorrelated and correlated input parameters", *Rock. Mech. Rock. Eng.*, **55**(5), 2787-2804. https://doi.org/10.1007/s00603-021-02697-4.

Sainoki, A., Tabata, S., Mitri, H.S., Fukuda, D. and Kodama, J. (2017), "Time-dependent tunnel deformations in homogeneous and heterogeneous weak rock formations", *Comput. Geotech.*, **92**, 186-200. https://doi.org/10.1016/j.compgeo.2017.08.008.

Sakcali, A. and Yavuz, H. (2019), "Estimation of radial deformations around circular tunnels in weak rock masses through numerical modelling", *Int. J. Rock. Mech. Min. Sci.*, **123**, 104092. https://doi.org/10.1016/j.ijrmms.2019.104092.

Shen, Q., Zheng, J.J., Cui, L., Pan, Y. and Cui, B. (2019), "A procedure for interaction between rock mass and liner for deep circular tunnel based on new solution of longitudinal displacement profile", *Eur. J. Environ. Civil. Eng.,* **26**(1), 280-298. https://doi.org/10.1080/19648189.2019.1657960.

Sheng, Y.M., Zou, J.F. and Chen, G.H. (2023), "Semianalytical solutions for elastic-brittle-plastic surrounding rock under biaxial in situ stress field based on unified strength criterion", *Int. J. Geomech*., **23**(10). https://doi.org/10.1061/IJGNAI.GMENG-8092.

Showkati, A., Salari-rad, H. and Aghchai, M.H. (2021). "Predicting long-term stability of tunnels considering rock mass weathering and deterioration of primary support", *Tunn. Undergr. Sp. Technol.*, **107**, 103670. https://doi.org/10.1016/j.tust.2020.103670.

Su, Y., Su, Y.H., Zhao, M.H. and Vlachopoulos, N. (2020), "Tunnel stability analysis in weak rocks using the convergence confinement method", *Rock. Mech. Rock. Eng.*, **54**(2), 559-582. https://doi.org/10.1007/s00603-020-02304-y.

Sun, Z.Y., Zhang, D.L., Fang, Q., Dui, G.S., Tai, Q.M. and Sun, F.W. (2021), "Analysis of the interaction between tunnel support and surrounding rock considering pre-reinforcement", *Tunn. Undergr. Sp. Technol.*, **115**, 104074. https://doi.org/10.1016/j.tust.2021.104074.

Sun, Z.Y., Zhang, D.L., Fang, Q., Wang, J.C., Chu, Z.F. and Hou, Y.J. (2023), "Analysis of interaction between tunnel support system and surrounding rock for underwater mined tunnels considering the combined effect of blasting damage and seepage pressure", *Tunn. Undergr. Sp. Technol.*, **141**, 105314. https://doi.org/10.1016/j.tust.2023.105314.

Wang, J., Li, E.B. and Chen, L. (2019), "Measurement and analysis of the internal displacement and spatial effect due to tunnel excavation in hard rock," *Tunn. Undergr. Sp. Technol.*, **84**, 151-165. https://doi.org/10.1016/j.tust.2018.11.001.

Wang, M.N., Wang, Z.L., Tong, J.J., Zhang, X., Dong, Y.C. and Liu, D.G. (2021), "Support pressure assessment for deep buried railway tunnels using BQ-index", *J. Cent. South. Uni.,* **28**(1), 247–263. https://doi.org/10.1007/s11771-021-4600-6.

Wang, Z.C., Shi, Y.F., Xie, Y.L., Zhang, M.Z., Liu, T. and Li, C., Zhang, C.P. (2021), "Support characteristic of a novel type of support in loess tunnels using the convergence-confinement method", *Int. J. Geomech*., **21**(10), 06021026. https://doi.org/10.1061/(ASCE)GM.1943-5622.0002094.

Wang, X.L. (2023), "A simple solution and dilatancy characterization for a circular tunnel excavated in the nonlinear strain-softening and nonlinear dilatancy rock mass", *Adv. Civ. Eng.*, **2023**, 3280223. https://doi.org/10.1155/2023/3280223.

Wong, L.N.Y., Fang, Q. and Zhang, D.L. (2013), "Mechanical analysis of circular tunnels supported by steel sets embedded in primary linings", *Tunn. Undergr. Sp. Technol.*, **37**, 80-88. https://doi.org/10.1016/j.tust.2013.03.011.

Xu, C., Xia, C.C. and Du, S.G. (2021), "Simplified solution for viscoelastic-plastic interaction between tunnel support and surrounding rock based on MC and GZZ strength criteria", *Comput. Geotech*., **139**, 104393. https://doi.org/10.1016/j.compgeo.2021.104393.

Yan, Q., Li, S.C., Xie, C. and Li, Y. (2018), "Analytical solution for bolted tunnels in expansive loess using the convergence-confinement method", *Int. J. Geomech*., **18**, 04017124. https://doi.org/10.1061/(ASCE)GM.1943-5622.0000989.

Ye, W.J., Wu, Y.T. and Chen, M. (2021), "Temporal and spatial effect of surrounding rock and supporting construction of a large soil tunnel", *Adv. Civil. Eng*., **2021**, 9962660. https://doi.org/10.1155/2021/9962660.

Zaheri, M., Ranjbarnia, M. and Dias, D. (2023), "New analytical approach to simulate the longitudinal fiberglass dowels performance installed at the face of a tunnel embedded in weak and weathered rock masses", *Comput. Geotech.*, **153**, 105080. https://doi.org/10.1016/j.compgeo.2022.105080.

Zaid, M. (2021), "Dynamic stability analysis of rock tunnels subjected to impact loading with varying UCS", *Geomech. Eng.*, **24**(6), 505-518. https://doi.org/10.12989/gae.2021.24.6.505.

Zareifard, M.R. (2020), "A new semi-numerical method for elastoplastic analysis of a circular tunnel excavated in a Hoek-Brown strain-softening rock mass considering the blast-induced damaged zone", *Comput. Geotech.*, **122**, 10103476.

Zhao, D., Jia, L., Wang, M. and Feng, W. (2016), "Displacement prediction of tunnels based on a generalised Kelvin constitutive model and its application in a subsea tunnel", *Tunn. Undergr. Sp. Technol*., **54**, 29-36. https://doi.org/10.1016/j.tust.2016.01.030.

Zhang, D.L. and Chen, L.P. (2016), "Compound structural characteristics and load effect of tunnel surrounding rock", *Chi. J. Rock. Mech. Eng.*, **35**, 456-469. (in Chinese) https://doi.org/10.13722/j.cnki.jrme.2015.0900.

Zhou, J. and Yang, X.A. (2021), "An analysis of the support loads on composite lining of deep-buried tunnels based on the Hoek-Brown strength criterion", *Tunn. Undergr. Sp. Technol.*, **118**, 104174. https://doi.org/10.1016/j.tust.2021.104174.

Zhou, J., Ding, Z., Huang, J.K., Yang, X.A. and Ma, M.J. (2024a), "The tunnel model tests of material development in different surrounding rock grades and the force laws in whole excavation-support processes", *Geomech. Eng.*, **36**(1), 51-69. https://doi.org/10.12989/gae.2024.36.1.051.

Zhou, J., Yang, X.A. and Ding, Z. (2023), "A secondary development based on the Hoek-Brown criterion for rapid numerical simulation prediction of mountainous tunnels in China", *Geomech. Eng.*, **34**(1), 69-86. https://doi.org/10.12989/gae.2023.34.1.069.

Zhou, J., Yang, X.A. and Ma, M.J. (2024b), "A new method for calculating the load shared by the primary support of deep-buried rheological soft rock tunnels by considering the flexible primary support", *Int. J. Appl. Mech.,* **16**(3). https://doi.org/10.1142/S1758825124500340.

IC